MIT Libraries | DSpace@MIT

MIT Open Access Articles

Diffusive Phonons in Nongray Nanostructures

The MIT Faculty has made this article openly available. ***Please share*** how this access benefits you. Your story matters.

Citation: Romano, Giuseppe and Alexie M. Kolpak. "Diffusive Phonons in Nongray Nanostructures." Journal of Heat Transfer 141, 1 (October 2018): 012401 © 2019 ASME

As Published: http://dx.doi.org/10.1115/1.4040611

Publisher: American Society of Mechanical Engineers (ASME)

Persistent URL: http://hdl.handle.net/1721.1/119823

Version: Final published version: final published article, as it appeared in a journal, conference proceedings, or other formally published context

Terms of Use: Article is made available in accordance with the publisher's policy and may be subject to US copyright law. Please refer to the publisher's site for terms of use.

Massachusetts Institute of Technology

Diffusive Phonons in Nongray Nanostructures

Giuseppe Romano
Department of Mechanical Engineering,
Massachusetts Institute of Technology,
77 Massachusetts Avenue,
Cambridge, MA 02139
e-mail: romanog@mit.edu

Alexie M. Kolpak
Department of Mechanical Engineering,
Massachusetts Institute of Technology,
77 Massachusetts Avenue,
Cambridge, MA 02139

Nanostructured semiconducting materials are promising candidates for thermoelectrics (TEs) due to their potential to suppress phonon transport while preserving electrical properties. Modeling phonon-boundary scattering in complex geometries is crucial for predicting materials with high conversion efficiency. However, the simultaneous presence of ballistic and diffusive phonons challenges the development of models that are both accurate and computationally tractable. Using the recently developed first-principles Boltzmann transport equation (BTE) approach, we investigate diffusive phonons in nanomaterials with wide mean-free-path (MFP) distributions. First, we derive the short MFP limit of the suppression function, showing that it does not necessarily recover the value predicted by standard diffusive transport, challenging previous assumptions. Second, we identify a Robin type boundary condition describing diffuse surfaces within Fourier's law, extending the validity of diffusive heat transport in terms of Knudsen numbers. Finally, we use this result to develop a hybrid Fourier/BTE approach to model realistic materials, obtaining good agreement with experiments. These results provide insight on thermal transport in materials that are within experimental reach and open opportunities for large-scale screening of nanostructured TE materials. [DOI: 10.1115/1.4040611]

Due to their ability to convert heat directly into electricity, thermoelectric (TE) materials have a wide range of applications, including waste heat recovery [1], wearable devices [2], and deep-space missions [3]. Widespread of TE materials is limited; however, by the simultaneous requirement for low thermal conductivity and high electrical conductivity, a condition that is rarely met in natural materials [4]. Nanostructured materials overcome this limitation in that heat-carrying phonons have mean free paths MFPs (Λ) larger than the limiting dimension, L_c, resulting in strong thermal transport suppression [5]. On the other side, electrons have MFPs that are typically as small as a few nanometers thus their size effects are mostly negligible [6]. Notable nanostructures, including thin films [7], nanowires [8,9], and porous materials [10–15], show a significant suppression in thermal conductivity with respect to the bulk, holding promises for high-efficiency thermal energy conversion.

In order to concisely describe phonon size effects in complex geometries, we have recently introduced the concept of "directional phonon suppression function," $S(\Lambda, \Omega)$. Such a quantity is proportional to the flux of phonons with mean-free-path (MFP) Λ and solid angle Ω traveling in the nanomaterial normalized to the thermal flux in the bulk counterpart [16]. The directionality of $S(\Lambda, \Omega)$ arises from the anisotropy in the geometry of the material. The effective thermal conductivity is then computed via $\kappa_{\text{eff}}/\kappa_{\text{bulk}} = \int_0^\infty d\Lambda \int_{4\pi} d\Omega K_{\text{bulk}}(\Lambda) S(\Lambda, \Omega)$, where $K_{\text{bulk}}(\Lambda)$ is the bulk MFP distribution, obtained from first-principles [17]. When averaged over the solid angle, $S(\Lambda, \Omega)$ reduces to the phonon suppression function, $\overline{S}(\Lambda)$ [16]. The suppression function, directly evaluated from the phonon Boltzmann transport equation (BTE), provides useful insights on thermal transport regimes [18,19]. We conveniently introduce the Knudsen number, defined as $\text{Kn} = \Lambda/L_c$. Phonons with large bulk Kn travel ballistically and their suppression function goas as $1/\Lambda$. On the other hand, the suppression of phonons with low Kns becomes independent on the MFP reaching a pleteau given by standard Fourier's law.

Using our recently developed solver for the space-dependent BTE, we investigate the diffusive limit of heat transport in materials with wide bulk MFP distributions, i.e., "nongray" materials. First, we provide an analytical expression for the small-Kn limit of the suppression function, demonstrating a significant departure from the gray model. Second, we investigate the effect of large-Kn phonons on the diffusive thermal flux along the wall of the pores, identifying a Robin-type boundary condition that, essentially, extends the range of validity of Fourier's law. Finally, using these two findings we implement a hybrid Fourier/BTE model to calculate κ_{eff} in realistic porous samples, obtaining good agreement with experiments. Our work enhance our knowledge of heat transport in nanostructured materials and provides insights for ab initio, multiscale thermal conductivity calculations.

In this work, we model phonon transport in nanostructured materials via the MFP-dependent BTE [18]

$$\Lambda \hat{\mathbf{s}}(\Omega) \cdot \nabla T(\mathbf{r}, \Lambda, \Omega) = T_L(\mathbf{r}) - T(\mathbf{r}, \Lambda, \Omega) \tag{1}$$

where $T(\mathbf{r}, \Lambda, \Omega)$ is an effective, space-dependent temperature associated with phonons with MFP Λ and direction $\hat{\mathbf{s}}(\Omega)$ denoted by Ω; the term $T_L(\mathbf{r})$ is an effective lattice temperature, obtained by

$$T_L(\mathbf{r}) = \int B_2(\Lambda) \overline{T}(\mathbf{r}, \Lambda, \Omega) d\Lambda \tag{2}$$

The term $B_2(\Lambda)$ is a bulk material property, computed by

$$B_n(\Lambda) = \left[\frac{K_{\text{bulk}}(\Lambda)}{\Lambda^n}\right] \left[\int \left(\frac{K_{\text{bulk}}(\Lambda')}{\Lambda'^n}\right) d\Lambda'\right]^{-1} \tag{3}$$

and $\overline{f}(\Omega) = \int_{4\pi}^{-1} d\Omega f(\Omega)$ is an angular average. Equation (2) results from the continuity equation for thermal flux, i.e., $\nabla \cdot \mathbf{J}(\mathbf{r}) = 0$. Within this formalism, the normalized thermal flux is $\mathbf{J}(\mathbf{r}, \Lambda, \Omega) = B_1(\Lambda) T(\mathbf{r}, \Lambda, \Omega) \hat{\mathbf{s}}(\Omega)$ [18], where we used the scaling factor $\left[\int K_{\text{bulk}}(\Lambda)/\Lambda d\Lambda\right]^{-1}$. For simplicity, when unambiguous, we will drop the space and angular dependencies from the notation.

Contributed by the Heat Transfer Division of ASME for publication in the Journal of Heat Transfer. Manuscript received October 16, 2017; final manuscript received June 12, 2018; published online October 8, 2018. Assoc. Editor: Alan McGaughey.

 Copyright © 2019 by ASME

Downloaded From: https://heattransfer.asmedigitalcollection.asme.org on 12/12/2018 Terms of Use: http://www.asme.org/about-asme/terms-of-use

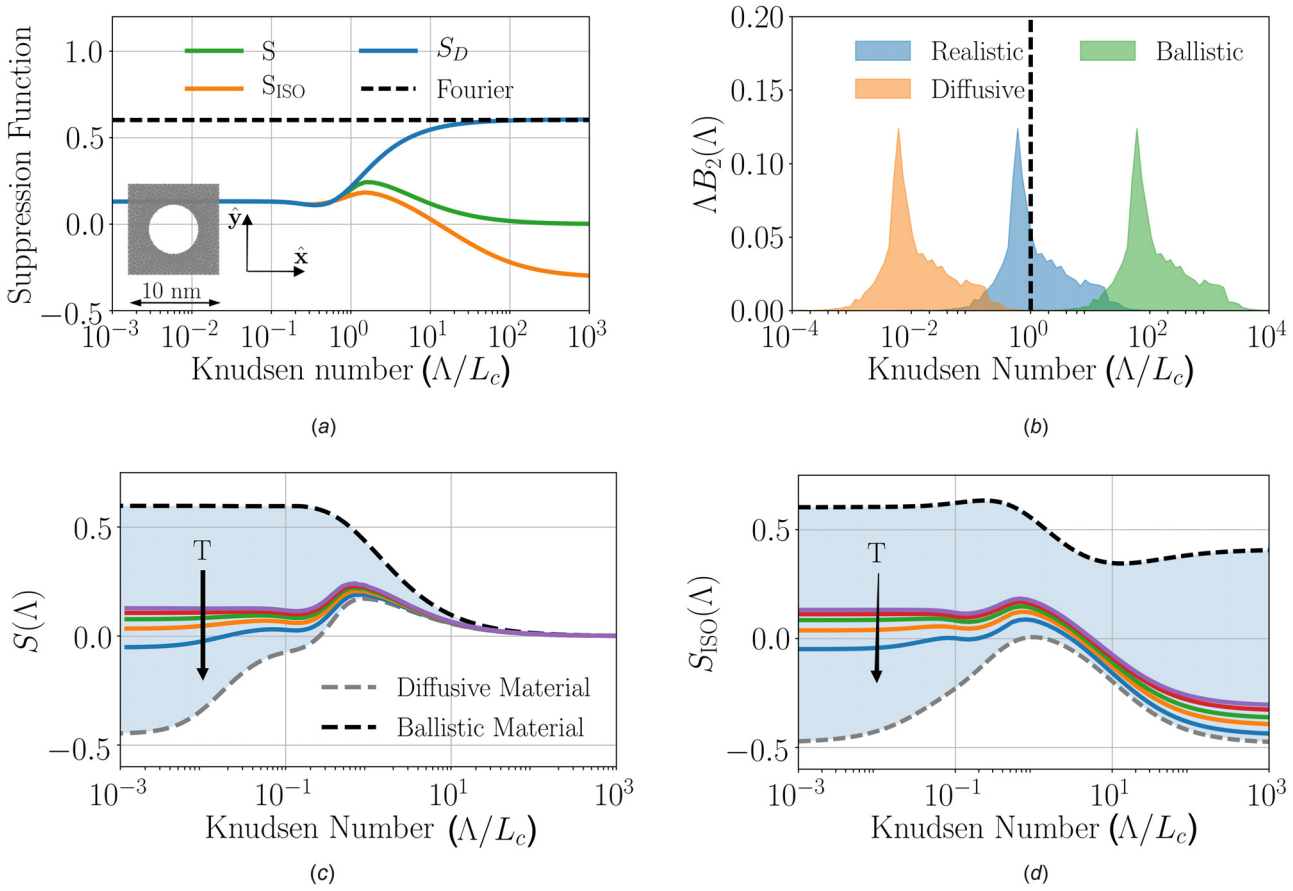

Fig. 1 (*a*) For short Kns, the suppression function, $\overline{S}(\Lambda)$, reaches a plateau that is significantly lower than that calculated by the standard Fourier's law. Up to Kn ≈ 1, the isotropic suppression function, $S_{ISO}(\Lambda) \approx \overline{S}(\Lambda)$, because the phonon distributions are isotropic. The diffusive suppression function, $S_D(\Lambda)$, reveals the breakdown of Fourier's law for Kn > 1. In the inset, the unit cell including a single circular pore and with periodicity $L = 10$ nm. (*b*) The coefficients $B_2(\Lambda)$ for a realistic, diffusive, and ballistic materials. The dotted line represents the characteristic length, L_c; (*c*) $S(\Lambda)$ and (*d*) $S_{ISO}(\Lambda)$ for the case of ballistic and diffusive materials. Realistic materials lie in the shaded regions. The curves for Si at $T = 150$, 200, 250, and 300 K are shown for comparison.

We first solve Eqs. (1) and (2) on ordered nanoporous Si with infinite thickness. As shown in Fig. 1(*a*), we consider a two-dimensional unit-cell containing one circular pore and apply periodic boundary conditions both along $\hat{\mathbf{x}}$ and $\hat{\mathbf{y}}$. We choose a porosity of $\varphi = 0.25$ and periodicity $L = 10$ nm. The walls of the pores are assumed to scatter phonons diffusively, a condition that translates into the following temperature imposed to outgoing phonons [20]:

$$T_B = \int B_1(\Lambda) g(\Lambda) d\Lambda \tag{4}$$

where $g(\Lambda)$ is the average flux of incoming phonons, given by $g(\Lambda) = [\langle \hat{\mathbf{s}} \cdot \hat{\mathbf{n}} \rangle_+]^{-1} \langle T(\Lambda) \hat{\mathbf{s}} \cdot \hat{\mathbf{n}} \rangle_+$. The notation $\langle f \rangle_+$ stands for an angular average for the hemisphere where $\hat{\mathbf{s}} \cdot \hat{\mathbf{n}} > 0$. Equation (4) arises from the condition of zero normal flux along the boundary. Heat flux is enforced by applying a difference of temperature $\Delta T = 1$ K between the hot and cold contacts, as illustrated in Fig. 1(*a*). Once Eqs. (1) and (2) are solved iteratively, we compute the directional suppression function [16]

$$S(\Lambda, \Omega) = -3 \frac{L}{\Delta T} \hat{\mathbf{s}} \otimes \hat{\mathbf{s}} \nabla \langle T(\Lambda) \rangle_{A_{hot}} \cdot \hat{\mathbf{n}} \tag{5}$$

where $\langle f \rangle_{A_{hot}} = (A_{hot})^{-1} \int_{A_{hot}} f dS$ is a spatial average along the hot contact, denoted by A_{hot}. In agreement with previous results [20], $\kappa_{eff} \approx 6\ \mathrm{Wm^{-1}K^{-1}}$, significantly lower than the bulk value $\kappa_{bulk} = \int K_{bulk}(\Lambda) d\Lambda \approx 153\ \mathrm{Wm^{-1}K^{-1}}$ [21]. The angularly averaged suppression function $\overline{S}(\Lambda)$, simply referred to as the suppression function, is shown in Fig. 1(*a*). We note that for large Kns, $\overline{S}(\Lambda) \propto 1/\Lambda$ in accordance with the ballistic regime, whereas suppression of phonons with short Kns is constant with MFP until approaching the quasi-ballistic regime, i.e., for Kn ≈ 1.

For small Kns, phonon distributions are isotropic and can be expanded to first-order spherical harmonics $T(\Lambda) \approx \overline{T}(\Lambda) - \Lambda \hat{\mathbf{s}} \cdot \nabla \overline{T}(\Lambda)$, which, when combined with Eq. (5) and after an angular average, leads to

$$\overline{S}_{ISO}(\Lambda) = -\frac{L}{\Delta T} \langle \nabla \overline{T}(\Lambda) \cdot \hat{\mathbf{n}} \rangle_{A_{hot}} \tag{6}$$

where ISO stands for "isotropic," and we used $\overline{\hat{\mathbf{s}} \otimes \hat{\mathbf{s}}} = (1/3)\delta_{ij}$. Heat transport in the short MFP region is calculated by including this expansion in Eq. (1), obtaining [22]

$$\frac{\Lambda^2}{3} \nabla^2 \overline{T}(\Lambda) = \overline{T}(\Lambda) - T_L \tag{7}$$

Equation (7) is the diffusive heat conduction equation with effective heat sources arising from the coupling between phonons with

Downloaded From: https://heattransfer.asmedigitalcollection.asme.org on 12/12/2018 Terms of Use: http://www.asme.org/about-asme/terms-of-use

different MFPs [22]. For $\Lambda \to 0$, Eq. (7) simplifies to $\overline{T}(0) = T_L$, which, after using Eqs. (2) and (6), gives

$$\overline{S}(0) = \int_0^\infty B_2(\Lambda) S_{\mathrm{ISO}}(\Lambda) d\Lambda \tag{8}$$

Equation (8) is the first key result of this paper. We note that $\overline{S}(0)$ depends on the entire bulk MFP distribution, embodying the effect of ballistic phonons on diffusive heat.

The upper bound of $\overline{S}(0)$ is evaluated by introducing the concept of "diffusive materials," i.e., a material where all the MFPs for which $B_2(\Lambda)$ is significant are much smaller than L_c, as depicted in Fig. 1(*b*). Under this condition, $T_L = \overline{T}(0)$, and Eq. (7) becomes the Laplacian $\nabla^2 \overline{T}(0) = 0$. Moreover, the boundary temperature becomes $T_B = \overline{T}(0)$. Then, $\overline{S}(0)$ is given by Eq. (6). For the case of ordered circular pores, this model gives $\overline{S}(0) \approx (1-\varphi)/(1+\varphi) = 0.6$, as illustrated in Fig. 1(*a*). This value can be seen as the diffusive limit of a diffusive material.

A lower limit to $\overline{S}(0)$ can be achieved in the case of a "ballistic material," namely when the MFPs contributing to $B_2(\Lambda)$ are much larger than L_c, as shown in Fig. 1(*b*). Within this regime, $T_B = g(\infty)$ and $\overline{S}(0) = -(L/\Delta T)\langle \nabla \overline{T}(\infty) \cdot \hat{\mathbf{n}} \rangle_{A_{\mathrm{hot}}} \approx -0.5$, with $\overline{T}(\infty)$ computed by Eq. (1). Although a negative suppression function is counterintuitive, note that the actual MFPs in the nanostructure $\Lambda_{\mathrm{nano}} = \overline{S}(\Lambda)\Lambda$ are still positive. Again, $\overline{S}_{\mathrm{ISO}}(0) = \overline{S}(0)$, because for short MFPs the phonon distributions are isotropic. Furthermore, $S_{\mathrm{ISO}}(0) = S_{\mathrm{ISO}}(\infty)$, as demonstrated by simply including $\overline{T}(\infty)$ in Eq. (5), and shown in Fig. 1(*d*). In the case of realistic materials $\overline{S}(\Lambda)$ and $S_{\mathrm{ISO}}(\Lambda)$ fall in between the diffusive and ballistic material limits, depending on the MFPs contributing to $B_2(\Lambda)$ with respect to L_c. In Figs. 1(*c*) and 1(*d*), we report $\overline{S}(\Lambda)$ and $S_{\mathrm{ISO}}(\Lambda)$, respectively, for different temperatures. We note that both functions decrease with temperature, as the bulk MFPs become larger [20], resulting in a shift of $B_2(\Lambda)$ toward higher MFPs.

We now analyze the effect of ballistic phonons on the boundary conditions along the boundary of the pore, within the diffusive regime. The condition imposed on phonons leaving the boundary, exemplified by Eq. (4), translates into the following expression for the angularly averaged, normal thermal flux:

$$\overline{\mathbf{J}}(\Lambda) \cdot \hat{\mathbf{n}} = \frac{1}{4} B_1(\Lambda) \left[g(\Lambda) - \int B_1(\Lambda') g(\Lambda') d\Lambda' \right] \tag{9}$$

where we used $\langle \hat{\mathbf{n}} \cdot \hat{\mathbf{s}} \rangle_+ = (1/4)$. The first and second terms in the parenthesis of Eq. (9) are related to the incoming and outgoing phonons, respectively, with respect to the boundary of the pore. To understand the power balance along the diffuse surface of the pore, we note that large Kn phonons tend to accumulate at the hot side of the pore wall [23], resulting in higher value of $g(\Lambda)$ with respect to diffusive phonons. Furthermore, as T_B is a weighted average of $g(\Lambda)$, we have $g(\Lambda > \mathrm{L}_c) > T_b > g(\Lambda < L_c)$, as illustrated in Fig. 2(*b*). Consequently, according to Eq. (9), the normal flux is positive for small Kns and negative for ballistic phonons (see Fig. 2(*a*)). The transition value is close to $\mathrm{Kn} = 1$ and depends on $B_1(\Lambda)$. The normal flux at the cold side of the pore has the opposite trend. To derive an approximation to Eq. (9) for short Kns, we first note that, within the diffusive regime, at a point right before the wall of the pore, heat flux is $\overline{\mathbf{J}}(\Lambda) = -B_1(\Lambda)\Lambda/3 \nabla \overline{T}(\Lambda)$. Then, we expand $g(\Lambda)$ up to its first harmonics, i.e., $g(\Lambda) = \overline{T}(\Lambda) - (2/3)\Lambda \nabla \overline{T}(\Lambda) \cdot \hat{\mathbf{n}}$, where we used $\langle \hat{\mathbf{s}} \otimes \hat{\mathbf{s}} \rangle_+ = (1/6)\delta_{ij}$. After combining these results, Eq. (9) becomes

$$\overline{\mathbf{J}}(\Lambda) \cdot \hat{\mathbf{n}} = \frac{1}{2} B_1(\Lambda) \left[\overline{T}(\Lambda) - T_B \right] \tag{10}$$

a typical Robin boundary condition for heat flux, with boundary conductance $(1/2)B_1(\Lambda)$. Equation (10) constitutes the second key result of this paper. In practice, the introduction of such a boundary condition extends the range of validity of Fourier's law to larger MFPs. To better visualize this concept, we introduce the "diffusive suppression function," $S_D(\Lambda)$, computed by Eq. (6) but with $\overline{T}(\Lambda)$ obtained with Eqs. (7)–(10) for the whole range of MFPs. From Fig. 1(*a*), we note a deviation from $\overline{S}(\Lambda)$ around $\mathrm{Kn} \approx 1$. The high-Kn limit of $S_D(\Lambda)$ is given by standard Fourier's law as Eq. (7) becomes the Laplacian of $\overline{T}(\Lambda)$.

In this last part, we calculate the thermal conductivity of recently fabricated porous Si membranes [14]. Among the available dataset, we consider the case with periodicity of 200 nm thickness of 145 nm and pores with diameters ranging from 90 nm through 168 nm. The bulk thermal conductivity, computed by the temperature dependent effective potential (TDEP) method [24,25], is $\kappa_{\mathrm{bulk}} \approx 142\ \mathrm{W\,m^{-1}\,K^{-1}}$. Although the solver for Eq. (1) has been conveniently parallelized, computing phonon transport in such a large simulation domain can become cumbersome. In particular, the computational bottleneck arises from the need to solve the BTE for a wide spectrum using the same space discretization. To this end, we devise a hybrid Fourier/BTE computational model that solves the BTE for long Kns phonons and Fourier's law (by means of Eqs. (7)–(10)) for phonons with small Kn. To uniquely define the MFP delimiting the two regions, we first solve both the BTE and Fourier model for decreasing MFP starting from the highest Λ in the bulk MFP distribution. Then,

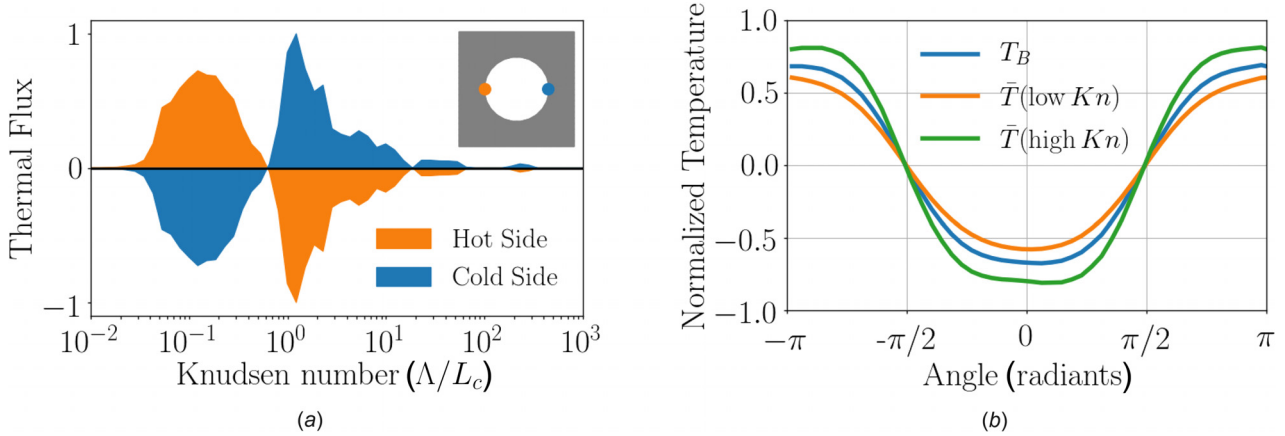

Fig. 2 (*a*) Normal thermal flux for different Kns at the hot and cold sides of the pore. (*b*) Temperature profile around the boundary of the pore for T_B, as calculated by Eq. (4), as well as for high and low Kn phonons. The angles $\phi = -\pi$ and $\phi = 0$ coincide with the directions $\hat{\mathbf{x}}$ and $-\hat{\mathbf{x}}$.

Downloaded From: https://heattransfer.asmedigitalcollection.asme.org on 12/12/2018 Terms of Use: http://www.asme.org/about-asme/terms-of-use

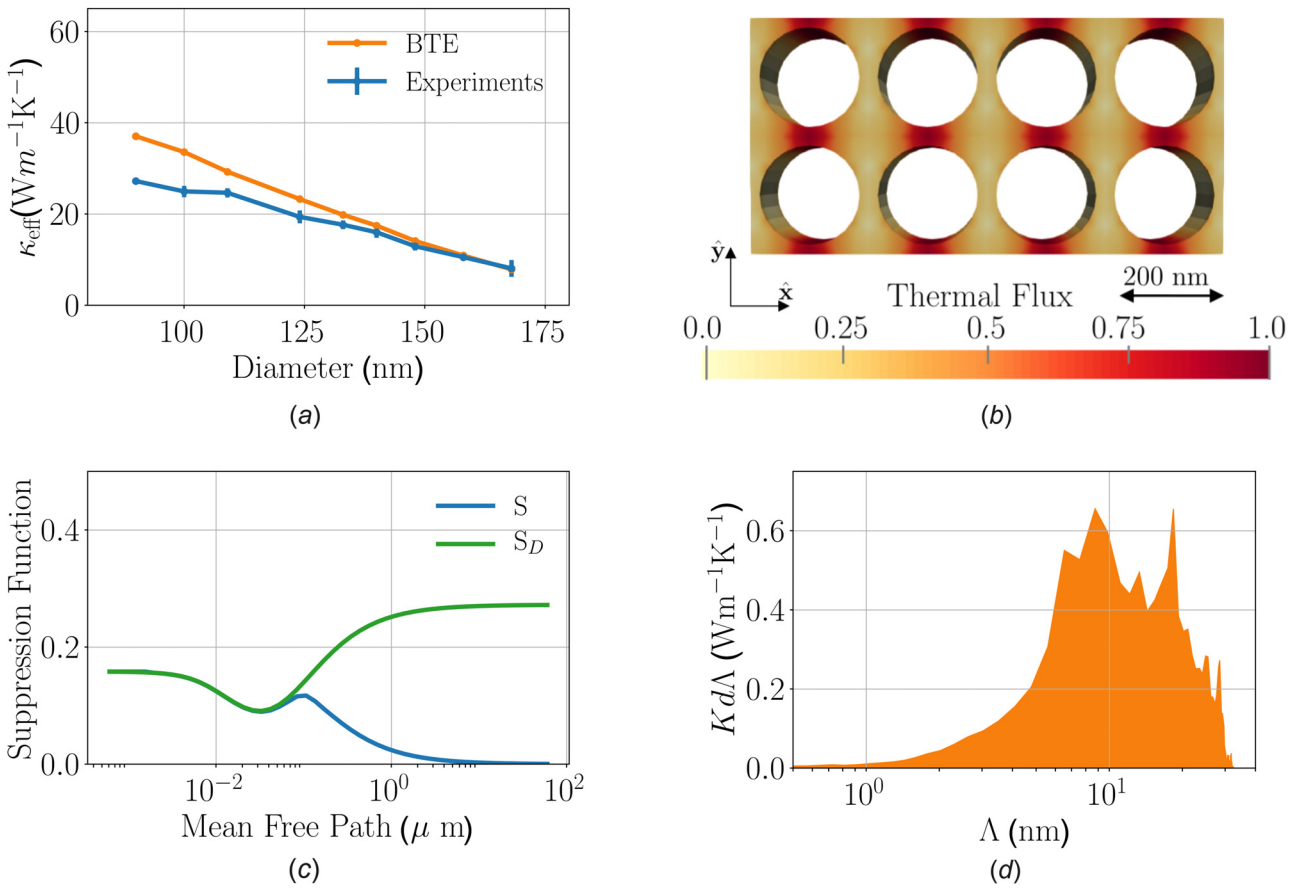

Fig. 3 (*a*) The effective thermal conductivity from calculations and experiments [14] and (*b*) the thermal flux profile. As expected, most of the heat travel along the space between pores along the temperature gradient. (*c*) The suppression function, $S(\Lambda)$ and the diffusive suppression function, $S_D(\Lambda)$. (*d*) The MFP distribution in the porous material. The maximum allowed MFP is around 30 nm, i.e., the phonon neck represented by the pore–pore distance.

when the resulting suppression functions converge within 1%, only the latter is used until a plateau for small Kns is obtained. In this case, the BTE is solved only for about 50% of the spectrum, allowing accurate phonon transport simulations within reasonable computational time. As shown in Fig. 3(*a*), the thermal conductivity decreases monotonically with the diameter until reaching the value of 7.4 $\text{Wm}^{-1}\text{K}^{-1}$ for the larger pore. Comparison with experiments show an excellent agreement for the case with small diameters and a qualitative agreement for large pores. Hereafter, all the results are for the case with a diameter of 168 nm. In Fig. 3(*b*), we illustrate the normalized thermal flux. Similarly to Ref. [18], most of the flux is concentrated along the space between pores, a typical signature of phonon size effects. Figure 3(*c*) shows $S(\Lambda)$ and $S_D(\Lambda)$. As these two functions are identical for a significant part of the low-MFP spectrum, we deduce that a large fraction of the heat travels diffusively. In Fig. 3(*d*), we report the MFP distribution $K_{\text{bulk}}\ (\Lambda S(\Lambda))S(\Lambda)$ in the membrane. We note that the maximum allowed MFP is around 30 nm, which is roughly the pore–pore distance.

In summary, using first-principles calculations and the BTE, we have rivisited the diffusive regime in nongray nanostructured materials. In particular, we investigated the effect of long-Kn phonons on heat diffusion, deriving an analytical expression for the short-Kn limit of the suppression function and a Robin type boundary condition for thermal flux normal to the pore boundaries. Finally, we developed a hybrid Fourier/BTE model to calculate the thermal conductivity in realistic materials, finding excellent agreement with experiments. These findings refine the concept of diffusive transport in nongray materials and pave the way for accurate yet inexpensive modeling of nanostructured materials for thermoelectric applications.

Acknowledgment

Research supported as part of the Solid-State Solar-Thermal Energy Conversion Center (S3TEC), an Energy Frontier Research Center funded by the U.S. Department of Energy (DOE), Office of Science, Basic Energy Sciences (BES), under Award DESC0001. We acknowledge Dr. Roman Anufriev for providing experimental data and Dr. Olle Hellman for providing the bulk thermal conductivity of Si, computed using the TDEP method.

Funding Data

- Office of Science (DESC0001).

References

[1] Bell, L. E., 2008, "Cooling, Heating, Generating Power, and Recovering Waste Heat With Thermoelectric Systems," Science, **321**(5895), pp. 1457–1461.
[2] Raihan, A., Siddique, M., Mahmud, S., and Van Heyst, B., 2017, "A Review of the State of the Science on Wearable Thermoelectric Power Generators (Tegs) and Their Existing Challenges," Renewable Sustainable Energy Rev., **73**, pp. 730–744.

Downloaded From: https://heattransfer.asmedigitalcollection.asme.org on 12/12/2018 Terms of Use: http://www.asme.org/about-asme/terms-of-use

[3] Ritz, F., and Peterson, C. E., 2004, "Multi-Mission Radioisotope Thermoelectric Generator (MMRTG) Program Overview," IEEE Aerospace Conference, Big Sky, MT, Mar. 6–13, pp. 2950–2957.
[4] Jeffrey Snyder, G., and Toberer, E. S., 2008, "Complex Thermoelectric Materials," Nat. Mater., **7**(2), pp. 105–114.
[5] Gang, C., 2005, *Nanoscale Energy Transport and Conversion: A Parallel Treatment of Electrons, Molecules, Phonons, and Photons*, Oxford University Press, Oxford, UK.
[6] Liao, B., Qiu, B., Zhou, J., Huberman, S., Esfarjani, K., and Chen, G., 2015, "Significant Reduction of Lattice Thermal Conductivity by the Electron-Phonon Interaction in Silicon With High Carrier Concentrations: A First-Principles Study," Phys. Rev. Lett., **114**(11), p. 115901.
[7] Venkatasubramanian, R., Siivola, E., Colpitts, T., and O'Quinn, B., 2001, "Thin-Film Thermoelectric Devices With High Room-Temperature Figures of Merit," Nature, **413**(6856), pp. 597–602.
[8] Hochbaum, A. I., Chen, R., Delgado, R. D., Liang, W., Garnett, E. C., Najarian, M., Majumdar, A., and Yang, P., 2008, "Enhanced Thermoelectric Performance of Rough Silicon Nanowires," Nature, **451**(7175), pp. 163–167.
[9] Boukai, A. I., Bunimovich, Y., Tahir-Kheli, J., Yu, J.-K., Goddard, W. A., III., and Heath, J. R., 2008, "Silicon Nanowires as Efficient Thermoelectric Materials," Nature, **451**(7175), pp. 168–171.
[10] Song, D., and Chen, G., 2004, "Thermal Conductivity of Periodic Microporous Silicon Films," Appl. Phys. Lett., **84**(5), pp. 687–689.
[11] Lee, J., Lim, J., and Yang, P., 2015, "Ballistic Phonon Transport in Holey Silicon," Nano Lett., **15**(5), pp. 3273–3279.
[12] Tang, J., Wang, H.-T., Lee, D. H., Fardy, M., Huo, Z., Russell, T. P., and Yang, P., 2010, "Holey Silicon as an Efficient Thermoelectric Material," Nano Lett., **10**(10), pp. 4279–4283.
[13] Hopkins, P. E., Reinke, C. M., Su, M. F., Olsson, R. H., Shaner, E. A., Leseman, Z. C., Serrano, J. R., Phinney, L. M., and El-Kady, I., 2011, "Reduction in the Thermal Conductivity of Single Crystalline Silicon by Phononic Crystal Patterning," Nano Lett., **11**(1), pp. 107–112.
[14] Verdier, M., Anufriev, R., Ramiere, A., Termentzidis, K., and Lacroix, D., 2017, "Thermal Conductivity of Phononic Membranes With Aligned and Staggered Lattices of Holes at Room and Low Temperatures," Phys. Rev. B, **95**(20), p. 205438.
[15] Alejandro, V.-F., Ryan A, D., Jeffrey K, E., John, C., Jeremy A, J., Peraud, J.-P. M., Lingping, Z., Zhengmao, L., Alexei A, M., Evelyn N, W., Alvarado-Gil, J. J., Sledzinska, M., Torres, C. M. S., Chen, G., and Nelson, K. A., 2016, "Thermal Transport in Suspended Silicon Membranes Measured by Laser-Induced Transient Gratings," AIP Adv., **6**(12), p. 121903.
[16] Romano, G., and Kolpak, A. M., 2017, "Directional Phonon Suppression Function as a Tool for the Identification of Ultralow Thermal Conductivity Materials," Sci. Rep., **7**, p. 44379.
[17] Broido, D. A., Malorny, M., Birner, G., Mingo, N., and Stewart, D. A., 2007, "Intrinsic Lattice Thermal Conductivity of Semiconductors From First Principles," Appl. Phys. Lett., **91**(23), p. 231922.
[18] Romano, G., and Grossman, J. C., 2015, "Heat Conduction in Nanostructured Materials Predicted by Phonon Bulk Mean Free Path Distribution," ASME J. Heat Transfer, **137**(7), p. 071302.
[19] Hua, C., and Minnich, A. J., 2014, "Transport Regimes in Quasiballistic Heat Conduction," Phys. Rev. B, **89**(9), p. 094302.
[20] Romano, G., Esfarjani, K., Strubbe, D. A., Broido, D., and Kolpak, A. M., 2016, "Temperature-Dependent Thermal Conductivity in Silicon Nanostructured Materials Studied by the Boltzmann Transport Equation," Phys. Rev. B, **93**(3), p. 035408.
[21] Li, W., Carrete, J., Katcho, N. A., and Mingo, N., 2014, "Shengbte: A Solver of the Boltzmann Transport Equation for Phonons," Comput. Phys. Commun., **185**(6), pp. 1747–1758.
[22] Loy, J. M., Murthy, J. Y., and Singh, D., 2013, "A Fast Hybrid Fourier–Boltzmann Transport Equation Solver for Nongray Phonon Transport," ASME J. Heat Transfer, **135**(1), p. 011008.
[23] Jeng, M.-S., Yang, R., Song, D., and Chen, G., 2008, "Modeling the Thermal Conductivity and Phonon Transport in Nanoparticle Composites Using Monte Carlo Simulation," ASME J. Heat Transfer, **130**(4), p. 042410.
[24] Hellman, O., and Abrikosov, I. A., 2013, "Temperature-Dependent Effective Third-Order Interatomic Force Constants From First Principles," Phys. Rev. B, **88**(14), p. 144301.
[25] Hellman, O., Abrikosov, I. A., and Simak, S. I., 2011, "Lattice Dynamics of Anharmonic Solids From First Principles," Phys. Rev. B, **84**(18), p. 180301.

Downloaded From: https://heattransfer.asmedigitalcollection.asme.org on 12/12/2018 Terms of Use: http://www.asme.org/about-asme/terms-of-use